Caging ruthenium complexes with non-toxic ligands for photoactivated chemotherapy

Cuello Garibo, J.A.

2

Influence of steric bulk and solvent on the photoreactivity of ruthenium polypyridyl complexes coordinated to L-proline

Here, the use of the natural amino acid L-proline as a protecting ligand for ruthenium-based PACT compounds is investigated in the series of complexes $[Ru(bpy)_2(L\text{-prol})]PF_6$ *(*$[\mathbf{1a}]PF_6$*, bpy = 2,2'-bipyridine, L-prol = L-proline),* $[Ru(bpy)(dmbpy)(L\text{-prol})]PF_6$ *(*$[\mathbf{2a}]PF_6$ *and* $[\mathbf{2b}]PF_6$*, dmbpy = 6,6'-dimethyl-2,2'-bipyridine), and* $[Ru(dmbpy)_2(L\text{-prol})]PF_6$ *(*$[\mathbf{3a}]PF_6$*). The synthesis of the tris-heteroleptic complex bearing the dissymmetric L-proline ligand yielded only two of the four possible regioisomers, called* $[\mathbf{2a}]PF_6$ *and* $[\mathbf{2b}]PF_6$*. Both isomers were isolated and characterized by a combination of spectroscopies and DFT calculations. The photoreactivity of all four complexes* $[\mathbf{1a}]PF_6$*,* $[\mathbf{2a}]PF_6$*,* $[\mathbf{2b}]PF_6$*, and* $[\mathbf{3a}]PF_6$*, was studied in water and acetonitrile using UV-visible spectroscopy, circular dichroism spectroscopy, mass spectrometry, and* ^1H *NMR spectroscopy. In water, upon visible light irradiation in presence of oxygen no photosubstitution took place, but the amine of complex* $[\mathbf{1a}]PF_6$ *was photooxidized to an imine. Contrary to expectations, enhancing the steric strain by addition of two (*$[\mathbf{2b}]PF_6$*) or four (*$[\mathbf{3a}]PF_6$*) methyl substituents did not lead, in phosphate buffered saline (PBS), to ligand photosubstitution. However, it prevented photoxidation, probably as a consequence of the electron-donating effect of the methyl substituents. In addition, whereas* $[\mathbf{2b}]PF_6$ *was photostable in PBS,* $[\mathbf{2a}]PF_6$ *quantitatively isomerized to* $[\mathbf{2b}]PF_6$ *upon light irradiation. In pure acetonitrile,* $[\mathbf{2a}]PF_6$ *and* $[\mathbf{3a}]PF_6$ *showed non-selective photosubstitution of both L-proline and dmbpy ligands, whereas the non-strained complex* $[\mathbf{1a}]PF_6$ *was photostable. Finally, in water-acetonitrile mixtures* $[\mathbf{3a}]PF_6$ *showed selective photosubstitution of L-proline, thus demonstrating the active role played by the solvent on the photoreactivity of this series of complexes. The role of solvent polarity, and coordination properties on the photochemical properties of polypyridyl complexes is discussed.*

This chapter was published as an Original Research paper: J. A. Cuello-Garibo, E. Pérez-Gallent, L. van der Boon, M. A. Siegler, and S. Bonnet, *Inorg. Chem.,* **2017**, *56*, 4818-4828.

2.1 Introduction

Due to their unique photophysical and photochemical properties, ruthenium polypyridyl complexes have found many applications in supramolecular chemistry,[1-6] molecular imaging,[7-11] chemical biology,[12-14] and medicinal chemistry.[15] Notably, several groups are studying the biological activity of ruthenium-based Photoactivated Chemotherapy (PACT) prodrugs.[16-20] These compounds are non-toxic or poorly toxic in the dark, but they become highly cytotoxic, or more cytotoxic, upon visible light irradiation. Unlike in Photodynamic Therapy (PDT), another phototherapeutic technique where phototoxicity comes from the light-induced generation of reactive oxygen species such as singlet oxygen, in PACT light activation occurs via an oxygen-independent mechanism that often relies on ligand photosubstitution reactions.[21] Ligand photosubstitution in polypyridyl complexes is typically attributed to the thermal promotion of photogenerated triplet metal-to-ligand charge-transfer (^{3}MLCT) excited states into dissociative, low-lying metal-centered triplet (^{3}MC) excited states. In many reported examples, ruthenium PACT compounds are based on complexes of the $[Ru(bpy)_3]^{2+}$ (bpy = 2,2'-bipyridine) family, where the photosubstituted ligand is a sterically hindering 2,2'-bipyridyl ligand such as 6,6'-dimethyl-2,2'-bipyridine (dmbpy).[19, 22,23] The increased cytotoxicity is generally attributed to the intracellular formation of the bis-aqua complex *cis*-$[Ru(bpy)_2(OH_2)_2]^{2+}$, which is believed to be the cytotoxic species. It should be noted, however, that upon light irradiation of $[Ru(bpy)_2(dmbpy)]^{2+}$ the free dmbpy ligand is also generated, which biological properties and cytotoxicity have not been evaluated yet.

In order to specifically address the question of the cytotoxicity of the metal-containing fragment, we embarked into investigating whether natural amino acids such as L-proline, instead of hindering bipyridyl ligands, could be used to cage a *cis* bis-aqua ruthenium species. Amino acids are naturally present in a cell, so that the photochemical generation of one equivalent of such ligands is not expected to have any impact on cell survival. For amino acid-caged ruthenium polypyridyl complexes, any light-induced toxicity would be solely attributed to the metal fragment. In literature several examples of *cis* ruthenium(II)-diimine complexes coordinated to deprotonated L-amino acids are described that, upon light irradiation, interconvert between the Λ-L and the Δ-L isomers.[24-25] However, to our knowledge, photosubstitution of an amino acid by solvent molecules has not been described yet. As reported for complexes with similar N,O chelating ligands,[26-28] the strong σ-donor properties of the carboxylate moiety usually increases the e_g level of the metal complex, and thereby the gap

between the ^{3}MLCT and ^{3}MC. Such increased gap enhances the photostability of the complex by quenching photosubstitution reactions involving the ^{3}MC states. In order to recover ligand photosubstitution properties, sterically hindering chelates such as dmbpy can be reintroduced, but if possible as spectator ligands, to see whether the ^{3}MC states are low enough in energy to come in the vicinity of that of the photochemically generated ^{3}MLCT states.[29]

Of course, octahedral complexes bearing chiral and/or dissymmetric bidentate ligands such as amino acids can lead to the formation of many different isomers.[30] Thus, the preparation of such complexes is *a priori* challenging, although diastereoselective coordination reactions making use of interligand repulsion and chromatographic separation techniques have been described in the past.[31-33] Here, we report on the synthesis of a series of L-proline-bound ruthenium complexes comprising Λ-[Ru(bpy)$_2$(L-prol)]PF$_6$ ([**1a**]PF$_6$), Λ-[Ru(bpy)(dmbpy)(L-prol)]PF$_6$ ([**2a**]PF$_6$ and [**2b**]PF$_6$), and Λ-[Ru(dmbpy)$_2$(L-prol)]PF$_6$ ([**3a**]PF$_6$, see Scheme 2.1). In this series, the number of sterically hindering methyl groups increases from zero in [**1a**]PF$_6$, to two in [**2a**]PF$_6$ and [**2b**]PF$_6$, and four in [**3a**]PF$_6$. The influence of the solvent on the photoreactivity of these complexes was also investigated.

2.2 Results and discussion

2.2.1 Synthesis and characterization

The four L-proline-coordinated ruthenium polypyridyl complexes were prepared as shown in Scheme 2.1. Complexes [**1a**]PF$_6$ and [**3a**]PF$_6$ were synthesized by reacting the precursor *rac*-[Ru(bpy)$_2$Cl$_2$] or *rac*-[Ru(dmbpy)$_2$Cl$_2$], respectively, with L-proline.[34] As reported by Meggers *et al.*, coordination of the chiral ligand L-proline to these racemic mixtures is diastereoselective and leads to the Λ-L diastereoisomer as the major ([**1a**]$^+$) or sole ([**3a**]$^+$) products.[34-36] The least strained complex was obtained as a 17:1 [**1a**]$^+$:[**1b**]$^+$ mixture of diastereoisomers, where [**1b**]$^+$ is the Δ-L isomer. This mixture can further be resolved by silica column chromatography to obtain analytically pure samples of [**1a**]PF$_6$. On the other hand, the most strained complex, [**3a**]PF$_6$, was directly obtained as a single Λ-L diastereoisomer without traces of the Δ-L diastereoisomer [**3b**]$^+$, as shown by the ^{1}H NMR of the crude product with a single set of 12 protons in the aromatic region.

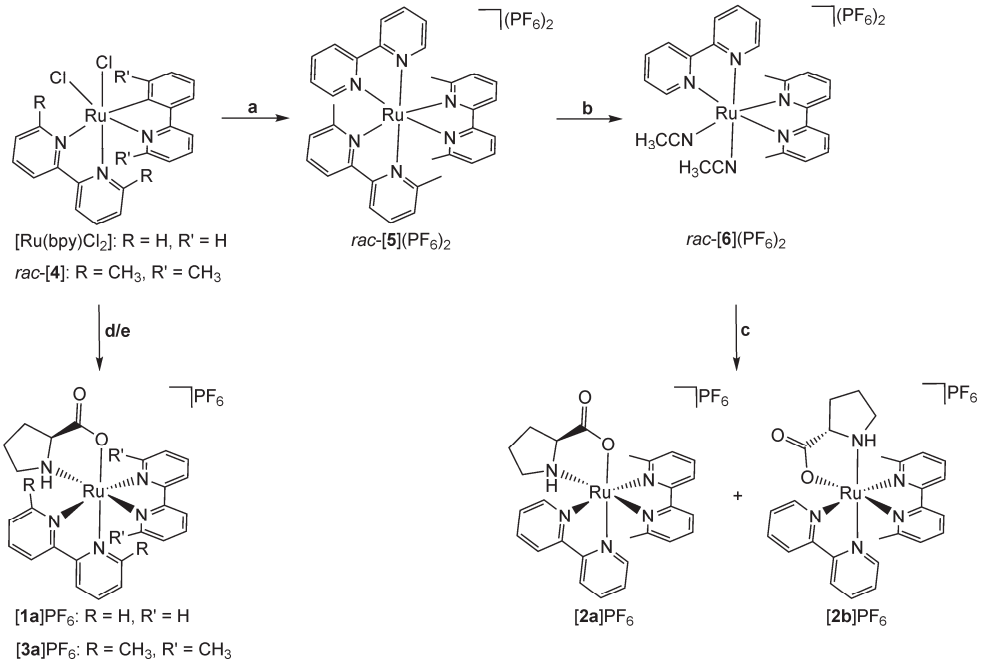

*Scheme 2.1. Synthesis of [**1a**]PF_6, [**2a**]PF_6, [**2b**]PF_6, and [**3a**]PF_6. a) i) rac-[**4**] (1 equiv), bpy (0.8 equiv), ethylene glycol, 3.5 h, 190 °C, pressure tube; ii) KPF_6, 79%; b) CH_3CN, 25 °C, White light Xe lamp, 59%; c) L-proline (2.5 equiv), K_2CO_3 (1.25 equiv), ethyene glycol, 40 min, 190 °C, pressure tube; d) [**1a**]PF_6 was synthesized according to Meggers et al.[34] e) i) rac-[**4**] (1 equiv), L-proline (2.2 equiv), K_2CO_3 (1.1 equiv), ethylene glycol, 45 min, 190 °C, pressure tube; ii) KPF_6, 56%.*

The tris-heteroleptic complexes [**2a**]PF_6 and [**2b**]PF_6 bear three different bidentate ligands and are less straightforward to prepare. Several methodologies to synthesize tris-heteroleptic polypyridyl ruthenium complexes are known in the literature, and most of them rely on the sequential addition of the different diimine ligands to a starting compound such as $[Ru(CO_2)_2Cl_2]_n$, *cis*-$[Ru(DMSO)_4Cl_2]$, or $[Ru(C_6H_6)Cl_2]_2$.[37-42] However, for the synthesis of the tris-heteroleptic complex bearing one dmbpy, [**2**]PF_6, we adapted a two-step synthesis introduced by von Zelewsky *et al.* using the highly strained $[Ru(bpy)(biq)_2]^{2+}$ species (biq = 2,2'-biquinoline) as an intermediate which, after irradiation in CH_3CN, leads to the tris-heteroleptic precursor $[Ru(bpy)(biq)(CH_3CN)_2]^{2+}$.[43] With this method we take advantage of the photoreactivity of strained ruthenium complexes and avoid the issues of adding a single equivalent of the first diimine ligand when other synthetic routes are used. Thus, as shown in Scheme 2.1, *rac*-$[Ru(dmbpy)_2Cl_2]$ (*rac*-[**4**]) was first converted into *rac*-$[Ru(bpy)(dmbpy)_2](PF_6)_2$ (*rac*-[**5**]$(PF_6)_2$) by addition of one equivalent of bpy in ethylene glycol at 190 ºC in a pressure tube. Limited ligand scrambling was observed,

resulting in a sample containing also *rac*-[Ru(dmbpy)$_3$](PF$_6$)$_2$ and *rac*-[Ru(bpy)$_2$(dmbpy)](PF$_6$)$_2$ as minor impurities (as observed by mass spectrometry, see Figure AIII.1). A solution of *rac*-[**5**](PF$_6$)$_2$ in CH$_3$CN was then irradiated using white light, whereby one dmbpy ligand was substituted by two solvent molecules to afford *rac*-[Ru(bpy)(dmbpy)(CH$_3$CN)$_2$](PF$_6$)$_2$ (*rac*-[**6**](PF$_6$)$_2$). Several impurities derived from ligand scrambling and their photolysis products were present as well at that stage (Figure AIII.2), but they could be for the most part removed after L-proline coordination. In the final step, L-proline was reacted with *rac*-[**6**](PF$_6$)$_2$ in ethylene glycol to yield the tris-heteroleptic complex [**2**]PF$_6$ in 62% yield as a mixture of isomers.

In octahedral complexes with two bpy or two dmbpy ligands and one L-proline the geometry is rather straightforward and only the two diastereoisomers Λ-L and Δ-L can exist. In contrast, for heteroleptic complexes with three different bidentate ligands the geometry is more complex: besides the chirality of the octahedron (Λ or Δ) and that of the proline ligand (here only L), which generates two diastereoisomers, the two possible orientations of the N,O dissymmetric proline ligand results in two different regioisomers. In other words, for the Λ-L and Δ-L isomers of [**2**]PF$_6$ either the amine group or the carboxylic acid moiety of L-proline is *trans* to dmbpy. The four possible diastereoisomers of [**2**]$^+$ are named [**2a**]$^+$, [**2b**]$^+$, [**2c**]$^+$, and [**2d**]$^+$, and their structures are shown in Figure AIII.20. According to ^{1}H NMR, the crude product [**2**]PF$_6$ was obtained, together with traces of [**3a**]PF$_6$, as a mixture of only two diastereoisomers in a ratio close to 1:1, as shown by the two characteristic doublets at 8.58 and 9.18 ppm corresponding to the position 6' on the bpy (Figure AIII.3). After purification by alumina chromatography using CH$_2$Cl$_2$:CH$_3$OH (CH$_3$OH = 1% to 3%) as an eluent, this mixture could be efficiently resolved. The first fraction was obtained as an NMR-pure sample whereas the second fraction was isolated as a mixture of a single isomer of [**2**]PF$_6$ and [**3a**]PF$_6$ in a ratio 85:15 (Figure AIII.3). Circular dichroism spectroscopy of these two isomers in H$_2$O showed a positive band at 300 nm for both isolated species (Figure AIII.4), which means that they both have the Λ octahedral configuration.[44-45] As a consequence, these isomers are necessarily complexes [**2a**]PF$_6$ and [**2b**]PF$_6$ (Figure AIII.20). NOESY analysis of the first fraction in D$_2$O showed an off-diagonal correlation between the α proton of the L-proline ligand and the methyl substituent on the dmbpy (Figure AIII.5), whereas no signal between those protons was found for the second fraction. Since the α proton and the methyl substituent on the dmbpy are closer in complex [**2a**]PF$_6$ than in complex [**2b**]PF$_6$, it is concluded that these complexes are

found in the first and the second fraction, respectively. Finally, single crystals suitable for X-ray structure determination were obtained for [**2b**]PF_6 by slow crystallization in water. The space group (P1) is chiral and the X-ray structure contained a single configuration of the coordination octahedron (Λ). The molecular structure, shown in Figure 2.1a, shows a long N5-C26 single bond (1.510(5) Å, Table 2.1) for the L-proline ligand, and the oxygen atom of L-proline is found *trans* to the dmbpy ligand. Thus, the nature of the isomer [**2b**]PF_6 is unequivocally confirmed, and as a consequence [**2a**]PF_6 was analysed as the Λ-L isomer having the oxygen *trans* to the bpy ligand.

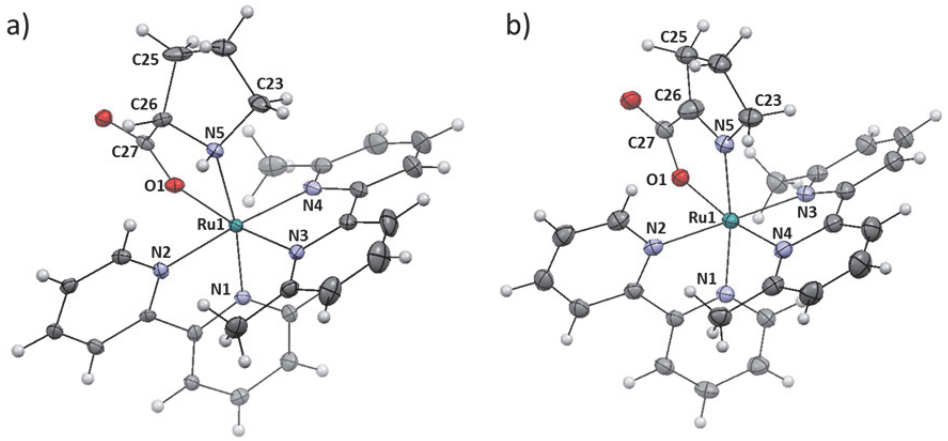

*Figure 2.1. Displacement ellipsoid plot (50% probability level) of the crystal structure of a) [**2b**]PF_6 and b) [**2b** – 2H]PF_6. Hexafluoridophosphate counteranions, lattice H_2O, and disorder have been omitted for clarity.*

*Table 2.1. Selected bond length (Å) and angles (°) for [**2b**]PF_6 and [**2b** − 2H]PF_6.*

	[2b]PF_6	[2b – 2H]PF_6
Ru1-O1	2.100(3)	2.111(1)
Ru1-N1	2.024(3)	2.047(1)
Ru1-N2	2.067(4)	2.066(2)
Ru1-N3	2.074(3)	2.074(2)
Ru1-N4	2.098(4)	2.067(2)
Ru1-N5	2.143(3)	2.046(1)
N5-C26	1.510(5)	1.305(3)
C25-C26-N5	115.5(2)	106.0(3)
C23-N5-C26-C27	122.1(4)	-174.4(2)

Density Functional Theory (DFT) calculations of both diastereoisomers Λ-L and Δ-L of $[\mathbf{1}]^+$ and $[\mathbf{3}]^+$, and the four possible diastereoisomers of $[\mathbf{2}]^+$, were performed in water using the COSMO model to simulate solvent effects (see Experimental section). The optimized structures, their energies in water, and their dipole moments are given in Figure AIII.20 and Table AIII.3, respectively. In water, the Λ complexes $[\mathbf{1a}]^+$ and $[\mathbf{3a}]^+$ are 6.9 and 19.6 kJ·mol^{-1} more stable than their Δ diastereoisomers $[\mathbf{1b}]^+$ and $[\mathbf{3b}]^+$, respectively. These results confirm that the diastereoselectivity of L-proline coordination to *rac*-$[Ru(bpy)_2Cl_2]$ or *rac*-$[Ru(dmbpy)_2Cl_2]$ is enhanced when hindering methyl substituents are put on the bpy ligands. For the heteroleptic complex $[\mathbf{2}]^+$, the isomer $[\mathbf{2b}]^+$ was found to be the most stable in water of all four isomers, followed by $[\mathbf{2a}]^+$, $[\mathbf{2d}]^+$, and $[\mathbf{2c}]^+$, at +1.9 kJ·mol^{-1}, +2.2 kJ·mol^{-1}, and +25.7 kJ·mol^{-1}, respectively. Although $[\mathbf{2c}]^+$ clearly is too high in energy to be formed under thermodynamic control, the isomers $[\mathbf{2a}]^+$, $[\mathbf{2b}]^+$, and $[\mathbf{2d}]^+$ are too close in energy to predict any stereoselectivity based on thermodynamic arguments. The fact that $[\mathbf{2d}]^+$ is not observed experimentally can be interpreted as a sign that the coordination of L-proline to $[Ru(bpy)(dmbpy)(CH_3CN)_2]^{2+}$ is under kinetic control. DFT models could also be used to find signs of steric hindrance in this series of complexes. The structural distortion parameters, *i.e.* the bond angle variance (σ^2) and the mean quadratic elongation (λ), were calculated for complexes $[\mathbf{1a}]^+$, $[\mathbf{2b}]^+$, and $[\mathbf{3a}]^+$ (Table AIII.4).[46-48] The values found, 50.5, 75.7, and 90.4 (σ^2), and $2.21\cdot10^{-4}$, $2.50\cdot10^{-4}$, and $3.06\cdot10^{-4}$ (λ), respectively, confirmed that addition of two or four methyl substituents at the 6 and 6' position of the bpy ligands has a major impact in the distortion of the octahedral geometry of the ruthenium complexes. Surprisingly, this distortion has no significant effect on the Ru-O bond distances, being 2.109, 2.105, and 2.109 Å in complexes $[\mathbf{1a}]^+$, $[\mathbf{2b}]^+$, and $[\mathbf{3a}]^+$, respectively.

2.2.2 Photochemistry

The photoreactivity of $[\mathbf{1a}]PF_6$ was studied first. The evolution of the UV-vis spectrum of a solution of $[\mathbf{1a}]PF_6$ in phosphate buffer saline (PBS) was studied upon irradiation at 493 nm under air. A hypsochromic shift in the ^{1}MLCT band was observed, with a change in the absorption maximum from 495 nm to 467 nm and an isosbestic point at 486 nm (Figure 2.2a). Mass spectrometry after irradiation showed a peak at m/z = 526.1 (Figure 2.3a), which is two units smaller than the starting complex (calcd m/z = 528.1). These two units correspond to the loss of two hydrogen atoms. According to Keene *et al.*, these hydrogens are dervied from the α-hydrogen and the amine hydrogen

of L-proline, *i.e.* the imine complex [Ru(bpy)$_2$(L-prol − 2H)]PF_6 ([**7**]PF_6) was formed.[49] A quantum yield (Φ_{PR}) of 0.0010 was calculated for this photoreaction in PBS (see Appendix I and Figure AI.3) and a dark control experiment at 37 ºC did not show any change in the UV-vis spectrum over time (Figure AIII.6), which excludes a thermal reaction. The oxidative nature of the photoreaction was confirmed by performing the same photoreaction under Ar. No change either in the UV-vis spectra (Figure 2.2b) or in the mass spectrum (Figure 2.3c) was observed in absence of molecular oxygen. When monitoring the irradiation with NMR under Ar, a new doublet appeared at 8.91 ppm, which corresponds to the Δ-L isomer [**1b**]$^+$ (Figure AIII.7).[34] In addition, a decrease in the band at 300 nm in the CD spectra was observed upon irradiation under the same conditions (Figure AIII.8), confirming the isomerization. Finally, addition of the antioxidant glutathione (GSH) before irradiation under air partially slowed down the photoreaction (Figure 2.2c and Figure AIII.9a). Under such conditions, mass spectrometry after 180 min of irradiation (Figure 2.3b) showed a mixture of [**1**]$^+$ (m/z = 528.1) and [**7**]$^+$ (m/z = 526.1), since the relative intensity of the peak at m/z = 528.1 in the isotopic pattern of [**7**]PF_6 was slightly higher than expected, as shown in the calculated isotopic pattern for a given 7:3 mixture of [**1**]$^+$:[**7**]$^+$ in Figure AIII.10.

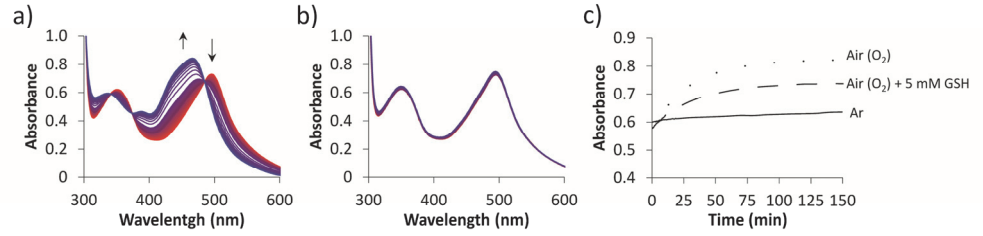

*Figure 2.2. Evolution of the UV-vis spectra of a 0.078 mM solution of [**1a**]PF_6 in PBS irradiated at 298 K with a 493 nm LED at a photon flux of $1.61 \cdot 10^{-7}$ mol·s^{-1} (a) under air and (b) under Ar. (c) Evolution of the Absorbance at 473 nm upon irradiation under air (dotted line), under air in presence of 5 mM GSH (dashed line), and under Ar (continuous line).*

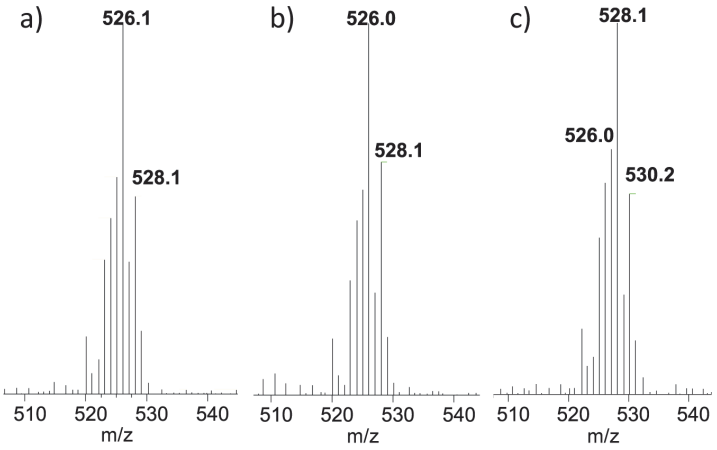

*Figure 2.3. Mass spectrum of a 0.078 mM solution of [**1a**]PF_6 in PBS after light irradiation at 298 K with a 493 nm LED at a photon flux of $1.61 \cdot 10^{-7}$ mol·s^{-1} (a) under air, (b), under air in presence of 5 mM GSH, and (c) under Ar. Conditions are detailed in Table AIII.1.*

In order to confirm that irradiation led to photooxidation and to compare our results under light irradiation to those obtained using electrochemical oxidation by Yamaguchi *et al.*,[50] a spectroelectrochemistry analysis of [**1a**]PF_6 was performed. Chronoamperometry of a solution of [**1a**]PF_6 in PBS with a constant potential of +0.645 V *vs*. Ag/AgCl using carbon sponges as working and counter electrodes was monitored with UV-vis spectroscopy. After 2 h, the current stabilized at 0.05 mA and the oxidative reaction was considered as finished. As shown in Figure AIII.18a and Figure AIII.19 the UV-vis and the mass spectra showed the same change as upon light irradiation, *i.e.* a hypsochromic shift from 495 nm to 466 nm in the MLCT band with an isosbestic point at 486 nm, and a peak at a m/z = 526.1. Thus, as shown in Scheme 2.2, upon light irradiation of [**1a**]$^+$ under Ar partial photoisomerization from Λ-L to Δ-L takes place, as has been described extensively in the literature for *cis*-ruthenium(II) diimine complexes coordinated to deprotonated amino acids.[24-25] However, in presence of O_2 the coordinated ligand L-proline is oxidized to its imine analogue [**7**]$^+$, as described for the complex $[Ru(bpy)_2(2\text{-}(L\text{-aminoethyl})(pyridine)](PF_6)_2$ by Keene *et al.* and for $[Os(bpy)_2(2\text{-aminoethanesulfinate})](PF_6)$ by Tamura *et al.*[49, 51] Although the exact mechanism of photooxidation is unclear, we suggest that the amine may be oxidized by the singlet oxygen ($^1O_2$) generated in presence of light and molecular oxygen, as it has been demonstrated that $^1O_2$ is a much better oxidant than the ground state $^3O_2$.[52] More in-depth studies would be needed to confirm this hypothesis.

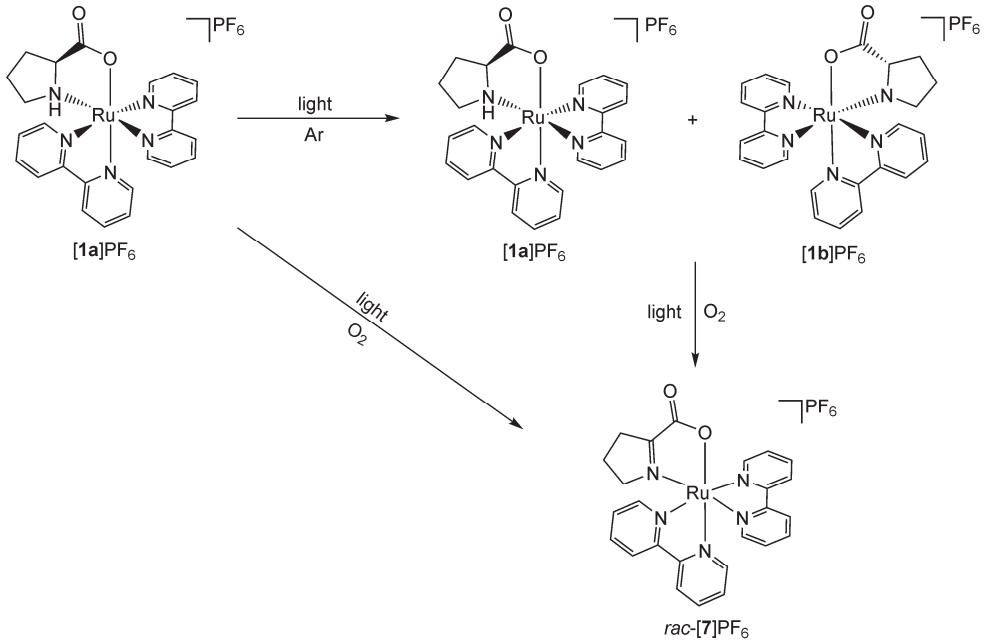

*Scheme 2.2. Scheme of the photoisomerization and photooxidation observed upon visible light irradiation of [**1a**]PF_6 in PBS at 298 K with a 493 nm LED at a photon flux of $1.61 \cdot 10^{-7}$ mol·s^{-1}.*

In a second step, the reactivity of the more strained complexes [**2a**]PF_6, [**2b**]PF_6, and [**3a**]PF_6, was investigated. When a solution of [**3a**]PF_6 was irradiated in PBS at 493 nm under air no change in the UV-vis or mass spectra was observed (Figure 2.4a and Figure AIII.9). Like for [**1a**]$^+$, partial isomerization from Λ-L to Δ-L occurred as shown by the decrease of the band at 300 nm in the CD spectrum (Figure AIII.11). Thus, for complex [**3a**]PF_6 photooxidation does not occur in PBS, which represents a dramatic change compared to the photoreactivity of [**1a**]PF_6. Surprisingly, despite the much higher steric hindrance of the complex, irradiation did not lead to photosubstitution reactions either. On the other hand, when a solution of [**2a**]PF_6 in deuterated PBS was irradiated with a 1000 W Xe lamp equipped with a 450 nm blue light filter and monitored with ^{1}H NMR, a doublet at 9.1 ppm, characteristic of the 6' proton of the bpy ligand in [**2b**]PF_6, arose upon 15 min irradiation. Under such conditions photoconversion of [**2a**]PF_6 to [**2b**]PF_6 was completed after 150 min irradiation (Figure 2.4b). By contrast, no change in the ^{1}H NMR spectrum was observed when irradiating [**2b**]PF_6 under the same conditions (Figure 2.4c). Thus, isomer [**2a**]PF_6, which is a kinetic product formed by coordination of L-proline to $[Ru(bpy)(dmbpy)(CH_3CN)_2]^{2+}$, isomerizes photochemically into [**2b**]PF_6, which is the thermodynamically most stable isomer of [**2**]$^+$. According to the UV-vis spectra evolution shown in Figure 2.4a, Figure

AIII.9b, and Figure AIII.9c, isomerization of [**2a**]$^+$ to [**2b**]$^+$ is not the only process occurring upon irradiation, and photooxidation takes place as well. However, this process occurs at a much lower rate than for [**1a**]$^+$.

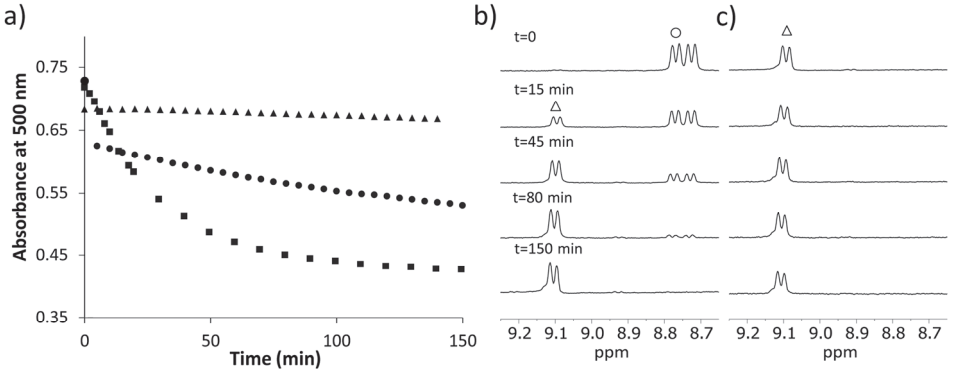

*Figure 2.4. a) Evolution of the absorption at 500 nm of a solution of [**1a**]PF_6 (0.078 mM, circles), [**2a**]PF_6 (0.032 mM, squares), and [**3a**]PF_6 (0.077 mM, triangles) in PBS upon irradiation under air with a 493 nm LED with a photon flux of $1.61 \cdot 10^{-7}$, $1.17 \cdot 10^{-7}$, and $1.48 \cdot 10^{-7}$ mol·s^{-1}, respectively. Conditions are detailed in Table AIII.1. b & c) Evolution of the ^{1}H NMR spectra of a solution of b) [**2a**]PF_6 (2.7 mg in 0.7 mL, circles) and c) [**2b**]PF_6 (2.6 mg in 0.7 mL, triangles) in deuterated PBS upon light irradiation with the beam of a 1000 W Xe lamp filtered with a 450 nm blue light filter under air.*

When a solution of [**2a**]PF_6 in water was left to slowly crystallize in presence of dimmed daylight, single crystals were obtained that could be analysed by X-ray crystallography. The crystal structure (Figure 2.1b) shows a short N5-C26 bond in the L-proline ligand (1.305(3) Å, Table 2.1) characteristic of a N=C double bond. Furthermore, the torsion angle between atoms C23-N5-C25-C27 is 174.4(2) in the new structure (*vs*. 122.1(4) in the crystal structure of [**2b**]PF_6), confirming the quasi-planar geometry of N5 and C26 in the new structure, and thus the oxidation of L-proline into an imine. In addition, the carboxylate O-donor group is found to be *trans* to dmbpy like in [**2b**]$^+$, which confirms the photochemical isomerization of [**2a**]$^+$ to [**2b**]$^+$ during crystallization. Thus, the obtained crystal structure corresponds to the imine complex [**2b** – 2H]$^+$. It should be noted that as this ruthenium complex crystallized in a space group that contained an inversion center (P-1), it is a racemate. Because NMR experiments showed that irradiation of [**2b**]$^+$ did not lead to the Δ isomer [**2d**]$^+$, finding both enantiomers in the crystal structure of [Ru(bpy)(dmbpy)(L-prol − 2H)]$(PF_6)\cdot H_2O$ means that the Λ-to-Δ racemization occurred after the photoisomerization of [**2a**]$^+$ to [**2b**]$^+$ *and* after photooxidation. According to Gomez *et al.*, the acidity of the amine of the coordinated L-proline ligand may have a crucial effect on the rate of

dehydrogenation for amino acids coordinated to polypyridyl ruthenium complexes.[53] The more acidic the amine, the faster the dehydrogenation takes place. In our case, the presence of more methyl substituents on the bpy ligands clearly leads to lower L-proline photoxidation rates. Since the methyl substituents are electron donating, a plausible interpretation of this observation is that more methyl substituents will thus increase the electron density on ruthenium and hence decrease the acidity of the coordinated L-proline amine. At that stage, however, it remains impossible to say whether or not the steric effects of the methyl groups contribute as well to the dramatic switch in photoreactivity observed in water between $[\mathbf{2a}]^+$, $[\mathbf{2b}]^+$, and $[\mathbf{3a}]^+$, and the non-strained complex $[\mathbf{1a}]^+$.

At that point, the absence of any photodissociation reaction upon irradiation of all four complexes in aqueous medium may be surprising, as the X-ray structure of $[\mathbf{2b}]^+$ and the DFT-minimized geometries of the strained molecules $[\mathbf{2a}]^+$, $[\mathbf{2b}]^+$, and $[\mathbf{3a}]^+$ are distorted enough to suggest the presence of low-lying ^{3}MC states. In order to investigate further this question, irradiation was performed in CH_3CN, which is a much less polar solvent than water, as well as an excellent ligand for ruthenium(II). When a CH_3CN solution of $[\mathbf{1a}]PF_6$ was irradiated at 493 nm under Ar no change in the maximum absorbance of the MLCT was observed (Figure 2.5). However, when the same experiment was performed using $[\mathbf{2a}]PF_6$, $[\mathbf{2b}]PF_6$, or $[\mathbf{3a}]PF_6$, a clear photoreaction was observed by UV-vis spectroscopy, characterized by a hypsochromic shift of the MLCT band of all three complexes (Figure 2.5). For the heteroleptic complex $[\mathbf{2a}]^+$, the maximum absorbance of the ^{1}MLCT band shifted from 509 nm to 432 nm (Figure 2.5b), and the mass spectrum after irradiation showed peaks at m/z = 185.4, 261.9, 452.2, and 669.2 (Figure AIII.12a). These peaks correspond to the free ligand $\{dmbpy + H\}^+$ (calcd m/z = 185.2), $[Ru(bpy)(dmbpy)(CH_3CN)_2]^{2+}$ (calcd m/z = 262.1), $[Ru(bpy)(L\text{-}Prol - 2H)(CH_3CN)_2]^+$ (calcd m/z = 452.1), and $\{[Ru(bpy)(dmbpy)(CH_3CN)_2]PF_6\}^+$ (calcd m/z = 669.1), respectively. Thus, in CH_3CN both bidentate ligands L-proline and dmbpy are photosubstituted by two solvent molecules. Similar results were found when a CH_3CN solution of $[\mathbf{3a}]PF_6$ was irradiated at 493 nm. A shift in the absorbance maximum of the MLCT band occurred from 516 nm to 444 nm (Figure 2.5d), and the mass spectrum after irradiation showed peaks at m/z = 185.5, 276.3, 480.2, and 697.2, corresponding to the free ligand $\{dmbpy+H\}^+$ (calcd m/z = 185.2), $[Ru(dmbpy)_2(CH_3CN)_2]^{2+}$ (calcd m/z = 276.1), $[Ru(dmbpy)(L\text{-}prol - 2H)(CH_3CN)_2]^+$ (calcd m/z = 480.1), and $\{[Ru(dmbpy)_2(CH_3CN)_2]PF_6\}^+$ (calcd m/z = 697.1), respectively (Figure AIII.12b).

Thus, also for $[\mathbf{3a}]^+$ irradiation in CH_3CN triggers the non-selective photosubstitution of both the L-proline and the dmbpy ligands. When the reaction was performed at a lower light intensity, the photosubstitution rate was lowered and a first isosbestic point at 493 nm could be observed during the first 10 min of the reaction (see Figure AIII.14a). A mass spectrum measured at that time point showed no peaks corresponding to free dmbpy (Figure AIII.14b), suggesting that L-proline is substituted more rapidly than dmbpy. Overall, in CH_3CN the strained complexes $[\mathbf{2a}]^+$ and $[\mathbf{3a}]^+$ indeed triggered the expected photosubstitution reactions that were not observed in PBS. However, these photoreactions are not selective and lead to the substitution of both L-proline and dmbpy.

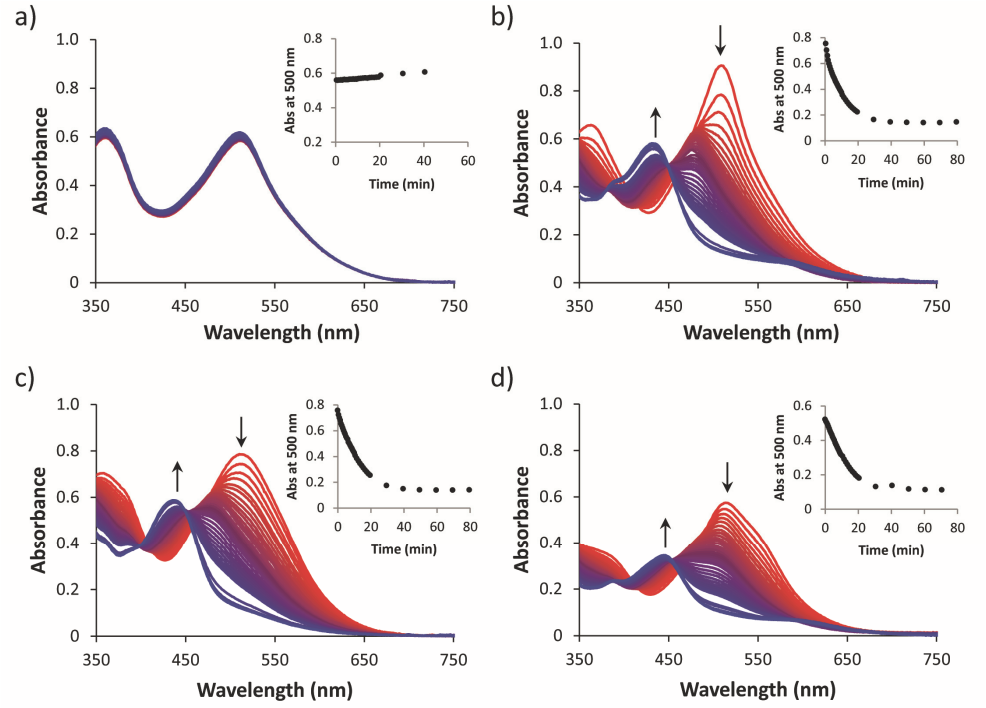

*Figure 2.5. a) Evolution of the UV-vis spectra of a solution of a) **[1a]**PF_6 (0.071 mM), b) **[2a]**PF_6 (0.092 mM), c) **[2b]**PF_6 (0.121 mM), and d) **[3a]**PF_6 (0.07 mM) in CH_3CN upon irradiation under Ar with a 493 nm LED with a photon flux of $1.10 \cdot 10^{-7}$, $1.12 \cdot 10^{-7}$, $1.05 \cdot 10^{-7}$, and $1.12 \cdot 10^{-7}$ mol·s^{-1}, respectively Conditions are detailed in Table AIII.1.*

Considering the discrepancy between the photoreactivity observed in aqueous buffer and that observed in CH_3CN, photosubstitution was also studied for $[\mathbf{3a}]^+$ in water mixtures containing large amounts (1 to 80 vol%) of CH_3CN, thus in pseudo first-order conditions. As shown in Figure AIII.15, in all cases photosubstitution occurred, as

demonstrated by an isosbestic point at 388 nm, two sequential isosbestic points at 457 and at 479 nm showing a two-stage reaction, and the overall shift of the maximum absorbance of the ^{1}MLCT band from 504 nm to 445 nm. Interestingly, mass spectra measured after the first stage of the reaction showed, next to the peaks at m/z = 275.8 and 697.5 corresponding to the final photoproduct $[Ru(dmbpy)_2(CH_3CN)_2]^{2+}$ (calcd m/z = 276.1) and $\{[Ru(dmbpy)_2(CH_3CN)_2]PF_6\}^+$ (calcd m/z = 697.1), an additional peak at m/z = 313.3 characteristic for an intermediate where one of the bidentate ligands is bound in a monodentate fashion and one CH_3CN is coordinated, *e.g.* $\{[Ru(dmbpy)_2(\eta^1\text{-L-prol})(CH_3CN)]^+ + H\}^{2+}$ (calcd m/z = 313.1, see Figure AIII.16). Mass spectrometry at the steady state neither showed this intermediate m/z = 313.3 peak, nor free dmbpy ligand. Clearly, the two-step photochemical reaction observed by UV-vis corresponds to the initial substitution of one coordinating atom of L-proline by one CH_3CN ligand, followed by the selective substitution of the second coordinating atom of L-proline by a second CH_3CN ligand. The absorbance of the solution at 500 nm evolved linearly with irradiation time during the first 5 min of all experiments, showing that under such conditions the reaction rate was constant (see Figure AIII.17a and Table AIII.2). Surprisingly, the observed rate constants (k_{obs}) for the formation of the final photoproduct $[Ru(dmbpy)_2(CH_3CN)_2]^{2+}$ evolved linearly with CH_3CN concentrations in water (Figure AIII.17b), which discards a fully dissociative mechanism for such two-step ligand photosubstitution. Since an associative mechanism is unlikely due to the crowdiness of the strained complex $[\mathbf{3a}]^+$, we suggest that the photosubstitution may take place *via* an interchange mechanism, although further kinetic studies should be performed to differenciate between a dissociative interchange and an associative interchange mechanism.[54-55] Overall, an important observation is that the selectivity of the photosubstitution reaction in a 2:8 H_2O:CH_3CN mixture was different from that observed in pure CH_3CN: in the former case photosubstitution was selective and only the L-proline ligand dissociated from the complex, whereas in the latter case both dmbpy and L-proline were photosubstituted.

The different photoreactivity of $[\mathbf{2a}]^+$, $[\mathbf{2b}]^+$, and $[\mathbf{3a}]^+$ in PBS, CH_3CN, and H_2O:CH_3CN mixtures is puzzling, but it may be rationalized by different hypotheses. First, the coordinating properties of CH_3CN molecules towards ruthenium(II) are better than that of H_2O. As the photosubstitution of L-proline or dmbpy seems to proceed *via* intermediates having η^1-coordinated bidentate ligands, more coordinating monodentate ligands may stabilize these intermediates, lowering overall activations barrier, and thus increasing photosubstitution rates in presence of CH_3CN. Second, the carboxylate

group of L-proline is highly polar and it has excellent hydrogen bond-accepting properties. Putative intermediates where L-proline is coordinated in η^1, κN fashion, may hence be stabilized in presence of water, which would enhance the rate of L-proline photosubstitution *vs.* that of dmbpy. In contrast, in CH_3CN these $[Ru(dmbpy)_2(\eta^1,\kappa N\text{-L-prol})]^+$ intermediates may be relatively destabilized, while photosubstitution of the less polar dmbpy ligands may occur *via* stabilized $[Ru(\eta^2\text{-dmbpy})(\eta^2\text{-L-prol})(\eta^1\text{-dmbpy})(CH_3CN)]^+$ intermediates. Finally, the different triplet excited states involved in photosubstitution reactions are stabilized to a different extend in polar *vs*. apolar solvents. ^{3}MLCT states are charge-transfer states that will be stabilized by solvents with a higher polarity (water), while ^{3}MC states are not charge-transfer excited states and will be less stabilized by high-polarity solvents. Thus, in water the ^{3}MLCT-^{3}MC energy gap should be larger compared to that in CH_3CN, and hence the rate of photosubstitution reactions will be lower. Low photosubstitution rates mean that slow photooxidation and photoisomerization reactions will be observed, whereas in pure CH_3CN photosubstititution outcompetes these processes. Thorough – and challenging – theoretical studies including triplet state modelling with explicit solvent molecules will be needed to evaluate the contribution of these three different effects on the solvent dependence of photosubstitution reactions.

2.3 Conclusions

In this work, we demonstrated that heteroleptic complexes bearing the dissymmetric N,O ligand L-proline can be prepared stereoselectively, isolated, and characterized. In complex [**1a**]$^+$ the absence of steric hindrance and the electron-rich oxygen ligand of L-proline prevents any photosubstitution reaction, both in chloride-containing aqueous solution and in CH_3CN. Instead, photooxidation occurs in presence of air, leading to the formation of a N=C double bond. In parallel, partial isomerization of the chiral ruthenium center from Λ to Δ occurs, as reported for other amino acidato analogues.[24] Increasing steric hindrance as in [**2a-b**]$^+$ and [**3a**]$^+$ did not promote photosubstitution in aqueous solution (PBS), unlike demonstrated with other ruthenium complexes such as $[Ru(bpy)_2(dmbpy)]^{2+}$ or $[Ru(tpy)(dmbpy)(L)]^{2+}$.[23, 56] Under such conditions, increasing the number of methyl groups on the bpy ligands strongly slows down photooxidation of the L-proline ligand, probably because of the electron-donating effect of the methyl groups. It was necessary to add an excess of CH_3CN in water to trigger the selective photosubstitution of L-proline in [**3a**]$^+$. In pure CH_3CN however, the increased strain in [**2a**]$^+$, [**2b**]$^+$, and [**3a**]$^+$ did promote photosubstitution reactions, but two ligands were photosubstituted in a non-selective fashion, *i.e.* L-proline *and* dmbpy. The influence of

the solvent on reactivity opens interesting mechanistic questions concerning photosubstitution reactions of ruthenium polypyridyl complexes. It also increases the complexity of the speciation of light-activatable anticancer compounds in cells. Photosubstitution reactions occurring in cells are usually modelled in aqueous, dichloromethane, or acetonitrile solutions, without discussing the difference between these media. Our results clearly demonstrate that solvents of different polarities and different coordinating properties may lead to different photoreactivities, and that choosing water *vs.* an organic solvent to study photosubstitution is not innocent. Finally, it may be noted that cellular microenvironments such as membranes, DNA, or protein binding pockets are rather hydrophobic, and that in such microenvironments photoreactions that seem not to occur in water, may actually take place.

2.4 Experimental

2.4.1 Materials and Methods

The ligands 2,2'-bipyridine (bpy), 6,6'-dimethyl-2,2'-bipyridine (dmbpy), and L-proline (L-prol) were purchased from Sigma-Aldrich, as well as monopotassium phosphate (KH_2PO_4), sodium chloride (NaCl), and *cis*-bis(2,2′-bipyridine)dichlororuthenium(II) hydrate (*cis*-[$Ru(bpy)_2Cl_2$]). Lithium chloride (LiCl) and potassium hexafluoridophosphate (KPF_6) were purchased from Alfar-Aesar and potassium carbonate (K_2CO_3) was obtained from Merck. All reactants and solvents were used without further purification. The synthesis of *cis*-[$Ru(dmbpy)_2Cl_2$] and [**1a**]PF_6 were carried out according to literature procedures.[34, 57] Sephadex LH-20 was used for the Size Exclusion Column (SEC).

Electrospray mass spectra (ES MS) were recorded by using a Thermoquest Finnagen AQA Spectrometer and a MSQ Plus Spectrometer, and CD spectra were recorded on a Bio-Logic MOS-500 spectrometer with a Bio-Logic ALX-300 lamp. For the irradiation experiments of NMR tubes, the light of a LOT 1000 W Xenon Arc lamp was used mounted with an infrared filter and either a 400 nm long pass or a 450 nm 450FS10-50 filter from Andover Corporation. UV-vis experiments were performed on a Cary 50 Varian spectrometer. When monitoring photoreactions with UV-vis, mass spectrometry, or circular dichroism (CD), a LED light source (λ_{ex} = 493 nm, with a Full Width at Half Maximum of 14 nm) with a photon flux between $1.08 \cdot 10^{-7}$ and $1.55 \cdot 10^{-7}$ $mol \cdot s^{-1}$ was used. For the spectroelectrochemistry a UV-vis light source

Avantes-DH-S-BAL and an Avantes Avaspec-2048 spectrometer were used. An Autolab PGSTAT101 potentiostat was used to perform the chronoamperometry.

All ^{1}H NMR spectra were recorded on Bruker DPX-300 or DMX-400 spectrometers. Chemical shifts are indicated in ppm relative to the residual solvent peak. For NMR experiments under Ar, NMR tubes with a PTFE stopper were used. For some NMR reactions a deuterated phosphate buffer saline (PBS) was used as a solvent. A 10 mM PBS with 110 mM NaCl was prepared by dissolving KH_2PO_4 (6.5 mg, 0.047 mmol), K_2HPO_4 (36.8 mg, 0.211 mmol), and NaCl (160.8 mg, 2.752 mmol) in D_2O (25 mL) to reach a final pH of 7.54 at 295 K. The pH was measured with a pH meter, taking into account that the measured pD = pH + 0.4.[58] For the rest of irradiations followed by UV-vis, MS, or CD, a 10 mM PBS with 110 mM NaCl was prepared by dissolving KH_2PO_4 (64.3 mg, 0.472 mmol) , K_2HPO_4 (353.6 mg, 2.030 mmol), and NaCl (1.605 g, 27.464 mmol) in Milli-Q water (250 mL) to reach a final pH of 7.35 at 295 K.

2.4.2 Synthesis

[Ru(bpy)$_2$(L-prol − 2H)]PF$_6$ ([**7**]PF$_6$). Synthesis of complex [**7**]PF$_6$ was adapted from a literature procedure.[50] Complex [**1a**]PF$_6$ (3.0 mg, 4.5 μmol) was dissolved in 50 mL PBS (pH 7.35) and transferred into one of the compartments of the two-compartment cell. Oxidation at constant potential of +0.645 V *vs*. Ag/AgCl reference electrode was carried out under Ar in a two-compartment cell with a nafion membrane. Carbon sponge electrodes were used as working and counter electrodes. Electrolysis was continued until the current stabilized. Then, complex [**7**]PF$_6$ was extracted with CH_2Cl_2 (3 × 20 mL) and dried over $MgSO_4$. After evaporation of the solvent by reduced pressure an orange solid was obtained. (2.8 mg, 93%). ^{1}H NMR (300 MHz, CD_3OD) δ 8.72 (d, J = 5.6 Hz, 1H), 8.66 (d, J = 8.1 Hz, 2H), 8.59 – 8.50 (m, 3H), 8.21 (dtd, J = 12.1, 7.9, 1.5 Hz, 2H), 7.97 – 7.70 (m, 5H), 7.57 (d, J = 5.8 Hz, 1H), 7.33 – 7.20 (m, 2H), 3.88 (s, 1H), 3.20 – 3.02 (m, 1H), 2.97 – 2.79 (m, 1H), 2.30 (m, 1H), 2.05 (m, 1H). ES MS m/z (calcd): 526.2 (526.1, $[M - PF_6]^+$).

***rac*-[Ru(bpy)(dmbpy)$_2$](PF$_6$)$_2$** (*rac*-[**5**](PF$_6$)$_2$). 2,2'-bipyridine (35 mg, 0.23 mmol, 0.8 equiv) and *rac*-[Ru(dmbpy)$_2$Cl$_2$] (150 mg, 0.28 mmol) were dissolved in ethylene glycol (5 mL), and the solution was deaereted by bubbling Ar for 30 min in a pressure tube. The tube was closed, put in a pre-heated oven at 190 ºC for 3.5 h, and then cooled down to RT. After addition of water (10 mL) and saturated KPF_6 aqueous solution (0.5 mL) an orange precipitate was obtained. The suspension was filtered and the precipitate was washed with cold water and cold ethanol. After drying under air an

orange powder was obtained (200 mg, 79%), which shows traces of ligand scrambling. ^{1}H NMR (300 MHz, CD_3CN) δ 8.46 (d, J = 8.0 Hz, 2H), 8.29 (d, J = 7.8 Hz, 2H), 8.14 (q, J = 8.3 Hz, 4H), 7.91 (td, J = 8.0, 1.4 Hz, 2H), 7.86 (d, J = 5.2 Hz, 2H), 7.72 (t, J = 7.9 Hz, 2H), 7.51 – 7.46 (m, 2H), 7.34 (ddd, J = 7.4, 5.9, 1.3 Hz, 2H), 7.07 (dd, J = 7.8, 0.9 Hz, 2H), 1.79 (s, 6H), 1.68 (s, 6H). ^{13}C NMR (75 MHz, CD_3CN) δ 167.80, 166.08, 160.54, 159.42, 158.52, 153.31, 139.49, 138.93, 138.15, 129.04, 128.18, 127.97, 124.56, 124.20, 123.52, 26.40, 25.45. ES MS m/z (calcd): 313.5 (313.1, $[M - 2\times PF_6]^{2+}$), 771.4 (771.1, $[M - PF_6]^+$).

***rac*-[Ru(bpy)(dmbpy)(CH$_3$CN)$_2$](PF$_6$)$_2$** (*rac*-[**6**](PF$_6$)$_2$). *rac*-[**5**](PF$_6$)$_2$ (150 mg, 0.16 mmol) was dissolved in a preparative irradiation cell in CH_3CN (110 mL). After deaereting the mixture by bubbling Ar for 20 min, the orange solution was irradiated with the beam of a 1000 W Xe lamp with both IR- and UV-cut-off filters. After 2 h irradiation, the solvent was removed under reduced pressure. The orange solid was re-dissolved in CH_3OH and purified by SEC in CH_3OH to remove free dmbpy ligand. After solvent evaporation an orange solid was obtained (84 mg, 59%). ^{1}H NMR (300 MHz, CD_3CN) δ 9.39 (ddd, J = 5.6, 1.5, 0.7 Hz, 1H), 8.38 (dt, J = 8.1, 1.1 Hz, 1H), 8.27 (dt, J = 8.0, 1.0 Hz, 2H), 8.20 (td, J = 7.9, 1.5 Hz, 1H), 8.14 – 8.06 (m, 2H), 7.93 (td, J = 7.9, 1.5 Hz, 1H), 7.82 – 7.66 (m, 4H), 7.52 (ddd, J = 5.7, 1.6, 0.8 Hz, 1H), 7.31 (ddd, J = 7.4, 5.7, 1.4 Hz, 1H), 7.12 (dd, J = 7.7, 1.3 Hz, 1H), 2.47 (s, 3H), 1.84 (s, 3H). ^{13}C NMR (75 MHz, CD_3CN) δ 167.33, 167.06, 159.84, 159.52, 159.39, 158.51, 155.64, 153.34, 139.36, 139.29, 138.87, 138.74, 128.30, 128.05, 127.97, 127.69, 124.64, 124.34, 122.53, 121.91, 27.23, 25.26, 4.74. ES MS m/z (calcd): 262.3 (262.1, $[M - 2\times PF_6]^{2+}$), 669.2 (669.1, $[M - PF_6]^+$).

[Ru(bpy)(dmbpy)(L-prol)]PF$_6$ ([**2**]PF$_6$). L-proline (25 mg, 0.22 mmol, 2.5 equiv), K_2CO_3 (15 mg, 0.11 mmol, 1.25 equiv), and *rac*-[**6**](PF$_6$)$_2$ (70.0 mg, 0.086 mmol) were dissolved in ethylene glycol (5 mL) and deaereted by bubbling Ar for 20 min in a pressure tube. The tube was closed and put in a pre-heated oven at 190 ºC. After 40 min at 190 ºC the reaction mixture was cooled down to RT, and most of the solvent was removed under high vacuum at 40 ºC. Then, the dark red paste was dissolved in water (15 mL) and extracted with CH_2Cl_2 (3 × 10 mL). The organic phases were combined and dried over $MgSO_4$, which was filtered. The solvent was then evaporated under reduced pressure and the solid was purified by an Alumina Chromatography column using a mixture CH_2Cl_2:CH_3OH 99:1 as eluent. Two main fractions were obtained from a long band (with an R_f around 0.35), which corresponded to the diastereoisomers [**2a**]PF$_6$ and [**2b**]PF$_6$:

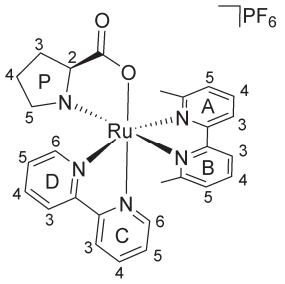

[**2a**]PF_6 (red solid, 19 mg, 31%) was isolated as 85% pure containing traces of [**3**]PF_6. ^{1}H NMR (500 MHz, D_2O) δ 8.76 (d, J = 5.6 Hz, 1H, D6), 8.73 (d, *J* = 5.7 Hz, 1H, C6), 8.52 (d, *J* = 8.1 Hz, 1H, D3), 8.41 (d, *J* = 8.2 Hz, 1H, C3), 8.22 (d, *J* = 8.1 Hz, 1H, A3), 8.14 – 8.09 (m, 2H, B3, D4), 7.96 (t, *J* = 8.0 Hz, 1H, A4), 7.85 (t, J = 8.0, 1H, C4), 7.70 (t, *J* = 7.9 Hz, 1H, B4), 7.67 – 7.63 (m, 1H, D5), 7.53 (d, *J* = 7.7 Hz, 1H, A5), 7.30 (td, *J* = 6.4, 5.8, 1.2 Hz, 1H, C5), 7.01 (d, *J* = 7.6 Hz, 1H, B5), 2.98 (s, 3H, AMe), 2.03 (q, *J* = 10.1 Hz, 1H, P3), 1.93 (dd, *J* = 11.2, 5.6 Hz, 1H, P5), 1.54 (td, *J* = 13.2, 12.1, 6.5 Hz, 1H, P3), 1.46 (dt, *J* = 13.1, 6.3 Hz, 1H, P4), 1.20 (s, 4H), 1.14 (tt, *J* = 11.3, 5.6 Hz, 1H, P5). ES MS m/z (calcd): 556.1 (556.1, $[M - PF_6]^+$), 584.0 (584.1 $[\mathbf{3}]^+$)

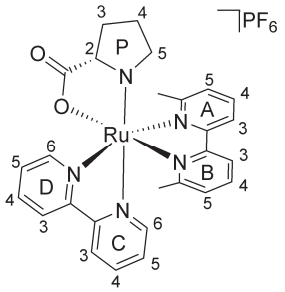

[**2b**]PF_6 (red solid, 8.1 mg, 13%) ^{1}H NMR (300 MHz, D_2O) δ 9.11 (d, *J* = 5.6 Hz, 1H, D6), 8.53 (d, *J* = 8.2 Hz, 1H, D3), 8.43 (d, *J* = 8.2 Hz, 1H, C3), 8.31 (d, *J* = 8.1 Hz, 1H, A3), 8.20 (d, *J* = 8.0 Hz, 1H, B3), 8.10 (m, 2H, C6/D4), 8.00 (t, *J* = 7.9 Hz, 1H, A4), 7.89 (dt, J = 7.8, 1.5 Hz, 1H, C4), 7.74 – 7.66 (m, 2H, A4/D5), 7.60 (d, *J* = 7.7 Hz, 1H, A5), 7.23 (ddd, *J* = 7.3, 5.7, 1.3 Hz, 1H, C5), 7.08 (d, *J* = 7.6 Hz, 1H, B5), 6.09 – 5.96 (m, 1H), 4.08 (q, *J* = 8.9 Hz, 1H), 2.55 (s, 4H), 2.23 (td, *J* = 10.0, 5.8 Hz, 1H), 1.62 (s, 3H), 1.55 – 1.34 (m, 2H), 1.30 – 1.16 (m, 1H). ES MS m/z (calcd): 556.1 (556.1, $[M - PF_6]^+$). UV-vis λ in nm (ε in $M^{-1}.cm^{-1}$): 511 (12300) in CH_3CN; 497 (9500) in PBS.

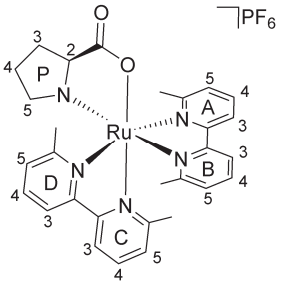

Λ-[Ru(dmbpy)$_2$(L-prol)]PF$_6$ ([**3a**]PF$_6$)**.** L-proline (22 mg, 0.19 mmol, 2.2 equiv), K_2CO_3 (13 mg, 0.094 mmol, 1.1 equiv), and *rac*-[Ru(dmbpy)$_2$Cl$_2$] (48 mg, 0.088 mmol) were dissolved in ethylene glycol (1 mL) and deaereted by bubbling Ar for 20 min in a pressure tube. The tube was closed and put in a pre-heated oven at 190 ºC and after 45 min the mixture was cooled down to RT. After addition of water (4 mL) and saturated KPF_6 aqueous solution (0.5 mL) a red precipitate was obtained. The suspension was filtered and the solid was washed with cold water and cold Et_2O. The red solid was purified by SEC in CH_3OH, obtaining a pure red solid (36 mg, 56%). ^{1}H NMR (300 MHz, CD_3OD) δ 8.45 – 8.35 (m, 3H, D3, A3, C3), 8.33 (d, J = 8.0 Hz, 1H, B3), 8.01 (m, 2H, A4, D4), 7.85 (td, J = 7.9, 1.9 Hz, 2H, B4, C4), 7.57 – 7.49 (m, 2H, D3, A5), 7.37 (dd, J = 7.5, 0.6 Hz, 1H, C5), 7.26 (d, J = 7.5 Hz, 1H, B5), 3.43 – 3.35 (m, 1H, P2), 2.88 (s, 3H, AMe), 2.48 (s, 3H, DMe), 2.14 (m, 1H, P5), 2.00 (s + m, 4H, CMe, P3), 1.66 (s + m, 4H, BMe, P3), 1.46 (m, 1H, P4), 1.34 (m, 1H, P4), 0.78 (qd, J = 11.4, 6.0 Hz, 1H, P5). High Resolution ES MS m/z (calcd): 584.15951 (584.16018, [M-PF$_6$]$^+$). Anal. Calcd for $C_{29}H_{32}F_6N_5O_2PRu$: C, 47.80; H, 4.43; N, 9.61 Found: C, 47.13; H, 4.41; N, 9.45. UV-vis λ in nm (ε in $M^{-1}.cm^{-1}$): 515 (7660) in CH_3CN.

2.4.3 Single Crystal X-Ray crystallography

Complex [2b]PF$_6$

Crystal growth: [**2b**]PF$_6$ (2.0 mg, 0.003 mmol) was dissolved in water (0.7 mL) in a GC vial. After two weeks, quality crystals suitable for X-ray structure determination were obtained.

X-ray structure: All reflection intensities were measured at 110(2) K using a SuperNova diffractometer (equipped with Atlas detector) with Mo Kα radiation (λ = 0.71073 Å) under the program CrysAlisPro (Version 1.171.36.32 Agilent Technologies, 2013). The temperature of the data collection was controlled using the system Cryojet (manufactured by Oxford Instruments). CrysAlisPro program was used

to refine the cell dimensions and for data reduction. The structure was solved by direct methods with SHELXS-2014/7 and was refined on F2 with SHELXL-2014/7.[59] Analytical numeric absorption correction based on a multifaceted crystal model was applied using CrysAlisPro. The H atoms were placed at calculated positions (unless otherwise specified) using the instructions AFIX 13, AFIX 23, AFIX 43 or AFIX 137 with isotropic displacement parameters having values 1.2 or 1.5 Ueq of the attached C or N atoms. The H atoms attached to O1W and O2W were found from difference Fourier map, and their coordinates were refined freely. The DFIX restraints were used to keep the O…H and H…H distances within acceptable ranges.

Details of the crystal structure: The structure is partly disordered**.** The asymmetric unit contains two crystallographically independent Ru molecules, two PF_6^- counterions, and two lattice water solvent molecules. Both PF_6^- counterions are disordered over two orientations, and the occupancy factors of the major components of the disorder refine to 0.52(3) and 0.777(9). Fw = 718.60, 0.43 × 0.14 × 0.03 mm^3, triclinic, *P1*, a = 8.5551(2), b = 9.6743(2), c = 17.6421(6), α = 87.003(2)°, β = 76.564(2)°, γ = 89.5481(19)°, V = 1418.22(7) $Å^3$, Z = 2, μ = 0.69 mm^{-1}, T_{min}–T_{max}: 0.805–0.981. 19350 reflections were measured up to a resolution of $(\sin \theta/\lambda)_{max}$ = 0.650 $Å^{-1}$. 11397 reflections were unique (R_{int} = 0.026), of which 10840 were observed [$I > 2\sigma(I)$]. 907 parameters were refined using 489 restraints. $R1/wR2$ [all refl.]: 0.028/0.065. S = 1.03. Residual electron density found between −0.62 and 0.63 e $Å^{-3}$.

Oxidized complex [2b – 2H]PF_6

Crystal growth: [**2a**]PF_6 (2.0 mg, 0.003 mmol) was dissolved in water (0.7 mL) into a GC vial and left in dimmed daylight. After six weeks, single crystals suitable for X-ray diffraction were obtained.

X-ray structure: All reflection intensities were measured at 110(2) K using a SuperNova diffractometer (equipped with Atlas detector) with Cu Kα radiation (λ = 1.54178 Å) under the program CrysAlisPro (Version 1.171.36.32 Agilent Technologies, 2013). The same program was used to refine the cell dimensions and for data reduction. The structure was solved with the program SHELXS-2014/7 and was refined on F2 with SHELXL-2014/7.[59] Analytical numeric absorption correction using a multifaceted crystal model was applied using CrysAlisPro. The temperature of the data collection was controlled using the system Cryojet (manufactured by Oxford Instruments). The H atoms were placed at calculated positions (unless otherwise specified) using the instructions AFIX 23, AFIX 43 or AFIX 137 with isotropic

displacement parameters having values 1.2 or 1.5 of the attached C atoms. The D atoms attached to O1W were found from difference Fourier maps, and their coordinates were refined freely.

Details of the crystal structure: The structure is ordered. Fw = 718.59, 0.33 × 0.15 × 0.059mm^3, triclinic, *P-1*, a = 8.5548(2), b = 11.6719(3), c = 14.8892(3), α = 93.9396(17)°, β = 92.7616(17)°, γ = 105.915(2)°, V = 1422.85(6) Å^3, Z = 2, μ = 5.71 mm^{-1}, T_{min}–T_{max}: 0.348–0.681. 18143 reflections were measured up to a resolution of (sin $\theta/\lambda)_{max}$ = 0.616 Å^{-1}. 5564 reflections were unique (R_{int} = 0.022), of which 5371 were observed [$I > 2\sigma(I)$]. 907 parameters were refined using 396 restraints. $R1/wR2$ [all refl.]: 0.025/0.061. S = 1.03. Residual electron density found between −0.76 and 0.68 e Å^{-3}.

2.4.4 Irradiation experiments monitored with ^{1}H NMR

Irradiation of [1a](PF$_6$): A stock solution of [**1a**]PF$_6$ in deuterated PBS (1.5 mg, 5 mL, 0.045 mM) was prepared and deaerated with Ar. Then, 650 µL were transferred, under Ar, into a NMR tube. The tube was irradiated at 310 K with a LOT Xenon 1000 W lamp equipped with IR short pass and >400 nm long pass filters. In addition, a control experiment without white light irradiation was performed, in which no reaction was observed after 5 hours. The reactions were monitored by ^{1}H NMR at various time intervals.

Irradiation of [2a](PF$_6$) and [2b](PF$_6$): [**2a**](PF$_6$) (2.7 mg) and [**2b**](PF$_6$) (2.6 mg) were weighed in two NMR tubes and dissolved in D_2O (0.7 mL in each tube). The tubes were irradiated at RT with a Xenon 1000 W lamp equipped with a 450 nm blue light filter 450FS10-50 from Andover Corporation. In addition, a control experiment without white light irradiation was performed, in which no reaction was observed after 5 hours. The reactions were monitored by ^{1}H NMR at various time intervals.

2.4.5 Irradiation experiments monitored with MS, UV-vis, and CD

UV-vis spectroscopy was performed using a UV-vis spectrometer equipped with temperature control set to 298 K and a magnetic stirrer. The irradiation experiments were performed in a quartz cuvette containing 3 mL of solution. A stock solution of the desired complex was prepared using either CH_3CN or PBS, which was then diluted in the cuvette to a working solution concentration. When the experiment was carried out under Ar the sample was deaereted 15 min by gentle bubbling of Ar and the

atmosphere was kept inert during the experiment by a gentle flow of Ar on top of the cuvette. A UV-vis spectrum was measured every 30 s for the first 10 min, every 1 min for the next 10 min, and eventually every 10 min until the end of the experiment. Data was analysed with Microsoft Excel. The quantum yield for the photooxidation of [**1a**]PF_6 in PBS was calculated by modelling the time evolution of the absorbance spectrum of the solution using the Glotaran software (see Appendix I and Figure AI.3).[60] Experimental conditions are detailed in Table AIII.1.

2.4.6 Spectroelectrochemistry

A solution of [**1a**]PF_6 in PBS (0.1 mM) was transferred into one of the compartments of a two-compartment cell separated by a nafion membrane, whereas the other compartment contained only PBS. Carbone sponges with a resistance lower than 10 mΩ were used as working and counter electrodes. An Ag/AgCl electrode in the main compartment was used as a reference electrode. Once the solution was deaerated by bubbling Ar for 15 min, the UV-vis probe was submerged into the working solution. The chronoamperometry was performed at a constant potential of +0.645 V vs. Ag/AgCl reference electrode taking points every second while UV-vis spectra were recorded every 2 min. When the current of the chronoamperometry was constant the experiment was terminated.

2.4.7 DFT calculations

Electronic structure calculations were performed using DFT as implemented in the ADF program (SCM). The structures of all possible isomers of [**1a**]$^+$, [**2b**]$^+$, and [**3a**]$^+$ were optimized in water using the conductor-like screening model (COSMO) to simulate the effect of solvent. The PBE0 functional and a triple zeta potential basis set (TZP) were used for all calculations.

2.4.8 Supporting information available

Appendix III: ^{1}H NMR spectra, mass spectra, and circular dichroism spectra of [**1a**]PF_6, [**2a**]PF_6, [**2b**]PF_6, and [**3a**]PF_6; UV-vis, mass spectrometry, circular dichroism, and ^{1}H NMR of the irradiation of [**1a**]PF_6, [**2a**]PF_6, [**2b**]PF_6, and [**3a**]PF_6; spectro-electrochemistry of [**1a**]PF_6; DFT calculations.

2.5 References

1. S. Bonnet, J. P. Collin, M. Koizumi, P. Mobian and J. P. Sauvage, *Adv. Mater.*, **2006**, 18, 1239-1250.
2. B. Champin, P. Mobian and J.-P. Sauvage, *Chem. Soc. Rev.*, **2007**, 36, 358-366.
3. J. Sauvage, J. Collin, J. Chambron, S. Guillerez, C. Coudret, V. Balzani, F. Barigelletti, L. De Cola and L. Flamigni, *Chem. Rev.*, **1994**, 94, 993-1019.
4. V. Balzani, G. Bergamini, F. Marchioni and P. Ceroni, *Coord. Chem. Rev.*, **2006**, 250, 1254-1266.
5. V. Balzani, P. Ceroni, A. Juris, M. Venturi, S. Campagna, F. Puntoriero and S. Serroni, *Coord. Chem. Rev.*, **2001**, 219, 545-572.
6. V. Balzani, A. Credi and M. Venturi, *Chem. Soc. Rev.*, **2009**, 38, 1542-1550.
7. V. Fernandez-Moreira, F. L. Thorp-Greenwood and M. P. Coogan, *Chem. Commun.*, **2010**, 46, 186-202.
8. A. Martin, A. Byrne, C. S. Burke, R. J. Forster and T. E. Keyes, *J. Am. Chem. Soc.*, **2014**, 136, 15300-15309.
9. M. R. Gill, J. Garcia-Lara, S. J. Foster, C. Smythe, G. Battaglia and J. A. Thomas, *Nat. Chem.*, **2009**, 1, 662-667.
10. M. R. Gill and J. A. Thomas, *Chem. Soc. Rev.*, **2012**, 41, 3179-3192.
11. L. Blackmore, R. Moriarty, C. Dolan, K. Adamson, R. J. Forster, M. Devocelle and T. E. Keyes, *Chem. Commun.*, **2013**, 49, 2658-2660.
12. J. Lee, D. G. Udugamasooriya, H.-S. Lim and T. Kodadek, *Nat. Chem. Biol.*, **2010**, 6, 258-260.
13. J. Y. Lee, P. Yu, X. S. Xiao and T. Kodadek, *Mol. BioSyst.*, **2008**, 4, 59-65.
14. J. Prakash and J. J. Kodanko, *Curr. Opin. Chem. Biol.*, **2013**, 17, 197-203.
15. C. Mari, V. Pierroz, S. Ferrari and G. Gasser, *Chem. Sci.*, **2015**, 6, 2660-2686.
16. K. T. Hufziger, F. S. Thowfeik, D. J. Charboneau, I. Nieto, W. G. Dougherty, W. S. Kassel, T. J. Dudley, E. J. Merino, E. T. Papish and J. J. Paul, *J. Inorg. Biochem.*, **2014**, 130, 103-111.
17. V. Lopes-dos-Santos, J. Campi, O. Filevich, S. Ribeiro and R. Etchenique, *Braz. J. Med. Biol. Res.*, **2011**, 44, 688-693.
18. J. Mosquera, M. I. Sanchez, J. L. Mascarenas and M. Eugenio Vazquez, *Chem. Commun.*, **2015**, 51, 5501-5504.
19. A. N. Hidayatullah, E. Wachter, D. K. Heidary, S. Parkin and E. C. Glazer, *Inorg. Chem.*, **2014**, 53, 10030-10032.
20. T. Respondek, R. N. Garner, M. K. Herroon, I. Podgorski, C. Turro and J. J. Kodanko, *J. Am. Chem. Soc.*, **2011**, 133, 17164-17167.
21. Y. Chen, W. Lei, G. Jiang, Y. Hou, C. Li, B. Zhang, Q. Zhou and X. Wang, *Dalton Trans.*, **2014**, 43, 15375-15384.
22. T. Sainuddin, M. Pinto, H. Yin, M. Hetu, J. Colpitts and S. A. McFarland, *J. Inorg. Biochem.*, **2016**, 158, 45-54.
23. B. S. Howerton, D. K. Heidary and E. C. Glazer, *J. Am. Chem. Soc.*, **2012**, 134, 8324-8327.
24. R. S. Vagg and P. A. Williams, *Inorg. Chim. Acta*, **1981**, 52, 69-72.
25. R. S. Vagg and P. A. Williams, *Inorg. Chim. Acta*, **1981**, 51, 61-65.
26. D. Leane and T. E. Keyes, *Inorg. Chim. Acta*, **2006**, 359, 1627-1636.
27. T. E. Keyes, J. G. Vos, J. A. Kolnaar, J. G. Haasnoot, J. Reedijk and R. Hage, *Inorg. Chim. Acta*, **1996**, 245, 237-242.
28. D. K. Heidary, B. S. Howerton and E. C. Glazer, *J. Med. Chem.*, **2014**, 57, 8936-8946.
29. Q. Sun, S. Mosquera-Vazquez, L. M. Lawson Daku, L. Guénée, H. A. Goodwin, E. Vauthey and A. Hauser, *J. Am. Chem. Soc.*, **2013**, 135, 13660-13663.
30. U. Knof and A. von Zelewsky, *Angew. Chem., Int. Ed.*, **1999**, 38, 302-322.
31. L. Gong, S. P. Mulcahy, K. Harms and E. Meggers, *J. Am. Chem. Soc.*, **2009**, 131, 9602-9603.
32. D. Hesek, Y. Inoue, S. R. L. Everitt, H. Ishida, M. Kunieda and M. G. B. Drew, *Chem. Commun.*, **1999**, 0, 403-404.

33. P. Hayoz, A. Von Zelewsky and H. Stoeckli-Evans, *J. Am. Chem. Soc.*, **1993**, 115, 5111-5114.
34. C. Fu, M. Wenzel, E. Treutlein, K. Harms and E. Meggers, *Inorg. Chem.*, **2012**, 51, 10004-10011.
35. T. J. Goodwin, P. A. Williams, F. S. Stephens and R. S. Vagg, *Inorg. Chim. Acta*, **1984**, 88, 165-181.
36. T. J. Goodwin, P. A. Williams and R. S. Vagg, *Inorg. Chim. Acta*, **1982**, 63, 133-140.
37. C. S. Burke and T. E. Keyes, *Rsc Advances*, **2016**, 6, 40869-40877.
38. D. Mulhern, S. Brooker, H. Gorls, S. Rau and J. G. Vos, *Dalton Trans.*, **2006**, 51-57.
39. D. A. Freedman, J. K. Evju, M. K. Pomije and K. R. Mann, *Inorg. Chem.*, **2001**, 40, 5711-5715.
40. M. Myahkostupov and F. N. Castellano, *Inorg. Chem.*, **2011**, 50, 9714-9727.
41. L. Spiccia, G. B. Deacon and C. M. Kepert, *Coord. Chem. Rev.*, **2004**, 248, 1329-1341.
42. P. A. Anderson, G. B. Deacon, K. H. Haarmann, F. R. Keene, T. J. Meyer, D. A. Reitsma, B. W. Skelton, G. F. Strouse and N. C. Thomas, *Inorg. Chem.*, **1995**, 34, 6145-6157.
43. A. von Zelewsky and G. Gremaud, *Helv. Chim. Acta*, **1988**, 71, 1108-1115.
44. B. Bosnich, *Inorg. Chem.*, **1968**, 7, 2379-2386.
45. B. Bosnich, *Inorg. Chem.*, **1968**, 7, 178-180.
46. K. Robinson, G. V. Gibbs and P. H. Ribbe, *Science*, **1971**, 172, 567-570.
47. M. E. Fleet, *Mineral. Mag.*, **1976**, 40, 531-533.
48. A. Dikhtiarenko, P. Villanueva-Delgado, R. Valiente, J. García and J. Gimeno, *Polymers*, **2016**, 8, 48.
49. F. R. Keene, M. J. Ridd and M. R. Snow, *J. Am. Chem. Soc.*, **1983**, 105, 7075-7081.
50. M. Yamaguchi, K. Machiguchi, T. Mori, K. Kikuchi, I. Ikemoto and T. Yamagishi, *Inorg. Chem.*, **1996**, 35, 143-148.
51. M. Tamura, K. Tsuge, A. Igashira-Kamiyama and T. Konno, *Chem. Commun.*, **2011**, 47, 12464-12466.
52. K. Krumova and G. Cosa, in *Singlet Oxygen: Applications in Biosciences and Nanosciences, Volume 1*, The Royal Society of Chemistry, **2016**, 1-21.
53. J. Gomez, G. Garcia-Herbosa, J. V. Cuevas, A. Arnaiz, A. Carbayo, A. Munoz, L. Falvello and P. E. Fanwick, *Inorg. Chem.*, **2006**, 45, 2483-2493.
54. E. Wachter and E. C. Glazer, *J. Phys. Chem. A*, **2014**, 118, 10474-10486.
55. S. Tachiyashiki and K. Mizumachi, *Coord. Chem. Rev.*, **1994**, 132, 113-120.
56. J. D. Knoll, B. A. Albani, C. B. Durr and C. Turro, *J. Phys. Chem. A*, **2014**, 118, 10603-10610.
57. J. P. Collin and J. P. Sauvage, *Inorg. Chem.*, **1986**, 25, 135-141.
58. A. Krężel and W. Bal, *J. Inorg. Biochem.*, **2004**, 98, 161-166.
59. G. M. Sheldrick, *Acta Crystallogr., Sect. C: Struct. Chem.*, **2015**, 71, 3-8.
60. J. J. Snellenburg, S. P. Laptenok, R. Seger, K. M. Mullen and I. H. M. van Stokkum, *J. Stat. Softw.*, **2012**, 49, 1-22.